A triply-responsive pillar[6]arene-based supramolecular amphiphile for tunable formation of vesicles and controlled release

Qizhong Zhou,* Huajiang Jiang, Rener Chen, Fangli Qiu, Guoliang Dai and Deman Han*

Department of Chemistry, Taizhou University, Taizhou 318000, P. R. China; Fax: +86-576-8866-0177; Tel: +86-576-8866-0177; E-mail: qizhongchou@tzc.edu.cn; hdm@tzc.edu.cn

Electronic Supplementary Information (20 pages)

1. Materials and methods

All reagents were commercially available and used as supplied without further purification. Solvents were either employed as purchased or dried according to procedures described in the literature. Compound **WP6**[S1] was synthesized according to published literature procedures. NMR spectra were recorded with a Bruker Avance DMX 400 spectrophotometer or a Bruker Avance DMX 500 spectrophotometer with the deuterated solvent as the lock and the residual solvent or TMS as the internal reference. Low-resolution electrospray ionization mass spectra (LRESI-MS) were obtained on a Bruker Esquire 3000 Plus spectrometer (Bruker-Franzen Analytik GmbH Bremen, Germany) equipped with an ESI interface and an ion trap analyzer. High-resolution electrospray ionization mass spectra (HRESI-MS) were obtained on a Bruker 7-Tesla FT-ICR mass spectrometer equipped with an electrospray source (Billerica, MA, USA). The melting points were collected on a SHPSIC WRS-2 automatic melting point apparatus. UV-vis spectroscopy was performed on a Shimadzu UV-2550 instrument at room temperature. The fluorescence experiments were conducted on a RF-5301 spectrofluorophotometer (Shimadzu Corporation, Japan). Energy-minimized structure was calculated using PM3 semiempirical molecular orbital methods (Frisch, M. J.; Trucks, G. W.; Schlegel, H. B.; Scuseria, G. E.; Robb, M. A.; Cheeseman, J. R.; Montgomery, J. A., Jr.; Vreven, T.; Kudin, K. N.; Burant, J. C.; Millam, J. M.; Iyengar, S. S.; Tomasi, J.; Barone, V.; Mennucci, B.; Cossi, M.; Scalmani, G.; Rega, N.; Petersson, G. A.; Nakatsuji, H.; Hada, M.; Ehara, M.; Toyota, K.; Fukuda, R.; Hasegawa, J.; Ishida, M.; Nakajima, T.; Honda, Y.; Kitao, O.; Nakai, H.; Klene, M.; Li, X.; Knox, J. E.; Hratchian, H. P.; Cross, J. B.; Adamo, C.; Jaramillo, J.; Gomperts, R.; Stratmann, R. E.; Yazyev, O.; Austin, A. J.; Cammi, R.; Pomelli, C.; Ochterski, J. W.; Ayala, P. Y.; Morokuma, K.; Voth, G. A.; Salvador, P.; Dannenberg, J. J.; Zakrzewski, V. G.; Dapprich, S.; Daniels, A. D.; Strain, M. C.; Farkas, O.; Malick, D. K.; Rabuck, A. D.; Raghavachari, K.; Foresman, J. B.; Ortiz, J. V.; Cui, Q.; Baboul, A. G.; Clifford, S.; Cioslowski, J.; Stefanov, B. B.; Liu, G.; Liashenko, A.; Piskorz, P.; Komaromi, I.; Martin, R. L.; Fox, D. J.; Keith, T.; Al-Laham, M. A.; Peng, C. Y.; Nanayakkara, A.; Challacombe, M.; Gill, P. M. W.; Johnson, B.; Chen, W.; Wong, M. W.; Gonzalez, C.; Pople, J. A. *Gaussian 03*, revision D.01; Gaussian, Inc.: Wallingford, CT, 2005).

*2. Synthesis of compound **AzoCh***

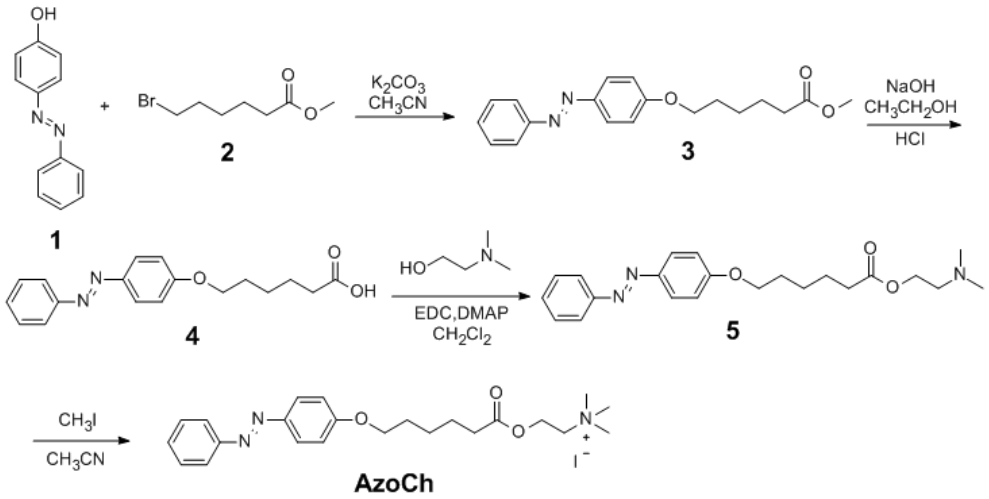

Scheme S1. Synthetic route to **AzoCh**.

Synthesis of 3. Methyl 6-bromohexanoate **2** (5.16 g, 20.0 mmol) and K_2CO_3 (6.62 g, 48.0 mmol) were added to a solution of *p*-Hydroxyazobenzene **1** (1.98 g, 10.0 mmol) in CH_3CN (100 mL). The mixture was heated in a three-necked flask under nitrogen atmosphere at reflux for 24 h. The cooled reaction mixture was filtered and washed with chloroform. The filtrate was evaporated under vacuum, and the residue was purified by flash column chromatography on silica gel (dichloromethane/petroleum ether = 1:5, *v*/*v*) to afford **3** as a red solid (2.97 g, 91%), mp 107.5−109.1 °C. The proton NMR spectrum of **3** is shown in Fig. S1. ^{1}H NMR (400 MHz, chloroform-*d*, room temperature) δ (ppm): 7.93−7.86 (m, 4H), 7.50 (t, J = 8.0 Hz, 2H), 7.43 (t, J = 8.0 Hz, 1H), 6.99 (d, J = 8.0 Hz, 2H), 4.04 (t, J = 8.0 Hz, 2H), 3.68 (s, 3H), 2.37 (t, J = 8.0 Hz, 2H), 1.88−1.81 (m, 2H), 1.76−1.69 (m, 2H), 1.57−1.49 (m, 2H). The ^{13}C NMR spectrum of **3** is shown in Fig. S2. ^{13}C NMR (100 MHz, chloroform-*d*, room temperature) δ (ppm): 174.09, 161.58, 152.79, 146.92, 130.32, 129.03, 124.75, 122.54, 114.69, 67.99, 51.55, 33.97, 28.88, 25.64, 24.67. LRESIMS is shown in Fig. S3: *m*/*z* 349.1 $[M + Na]^+$ (100%). HRESIMS: *m*/*z* calcd for $[M + H]^+$ $C_{19}H_{22}N_2O_3Na$, 349.3896, found 349.3905, error 2.6 ppm.

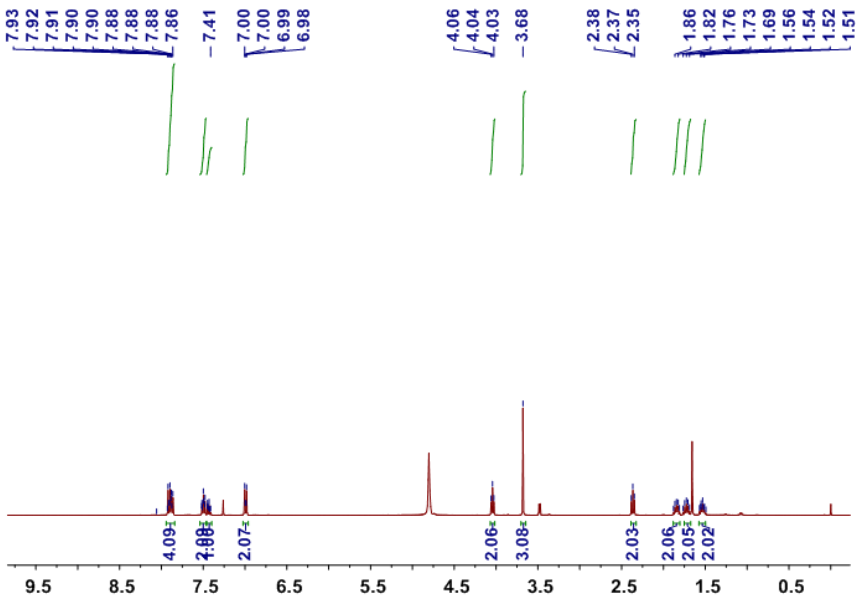

Fig. S1 ^{1}H NMR spectrum (400 MHz, chloroform-*d*, 293K) of **3**.

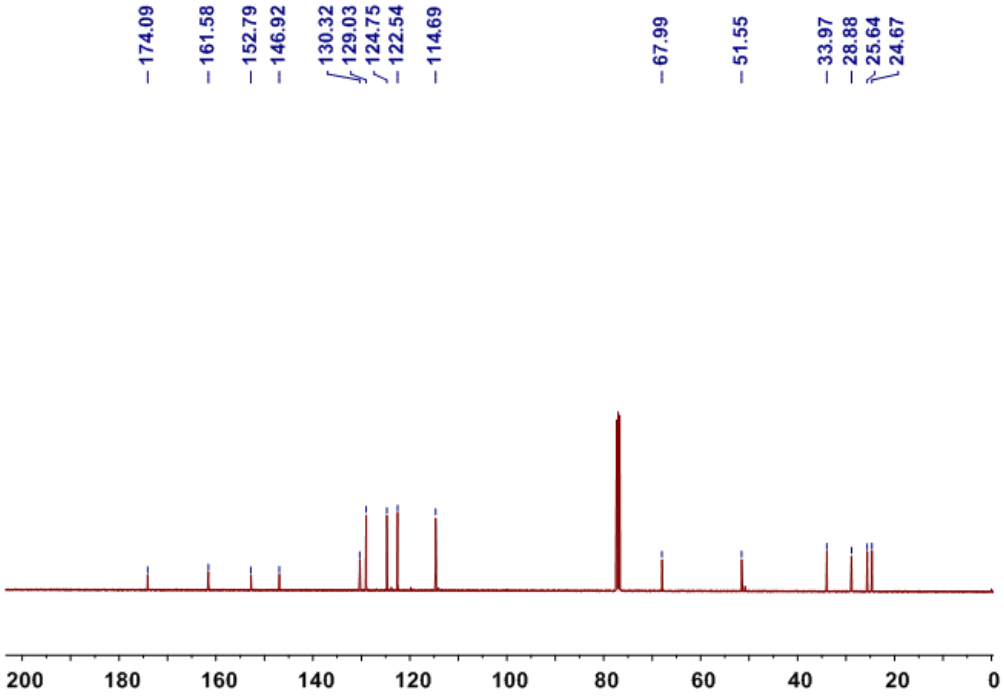

Fig. S2 ^{13}C NMR spectrum (100 MHz, chloroform-*d*, 293K) of **3**.

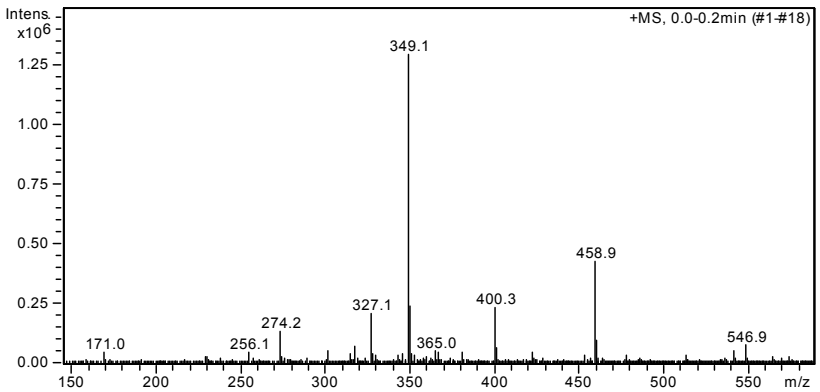

Fig. S3 Electrospray ionization mass spectrum of **3**. Assignment of the main peak: *m*/*z* 349.1 $[M + Na]^{+}$.

Synthesis of 4. A solution of **3** (1.23 g, 5.00 mmol) in CH_3CH_2OH (40 mL) was treated with 40% aqueous sodium hydroxide (80 mL) at reflux for 12 h. The mixture was concentrated under reduced pressure, diluted with water (10 mL), and acidified with HCl. The precipitated product **4** was collected by filtration, washed with water and dried under vacuum as a red solid (1.40 g, 90%), mp 104.7−106.1 °C. The proton NMR spectrum of **4** is shown in Fig. S4. ^{1}H NMR (400 MHz, DMSO-d_6, room temperature) δ (ppm): 7.89–7.83 (m, 4H), 7.57 (t, J = 8.0 Hz, 2H), 7.53 (t, J = 8.0 Hz, 1H), 7.13 (d, J = 8.0 Hz, 2H), 4.06 (t, J = 8.0 Hz, 2H), 1.86 (t, J = 8.0 Hz, 2H), 1.75–1.71 (m, 2H), 1.50–1.45 (m, 2H), 1.40–1.36 (m, 2H). The ^{13}C NMR spectrum of **4** is shown in Fig. S5. ^{13}C NMR (100 MHz, DMSO-d_6, room temperature) δ (ppm): 178.97, 161.55, 152.77, 146.91, 130.35, 129.05, 124.77, 122.55, 114.68, 67.94, 33.78, 28.88, 25.58, 24.41. LRESIMS is shown in Fig. S6: m/z 310.9 $[M - H]^-$ (100%). HRESIMS: m/z calcd for $[M - H]^-$ $C_{18}H_{19}N_2O_3$, 311.3630, found 311.3635, error 1.6 ppm.

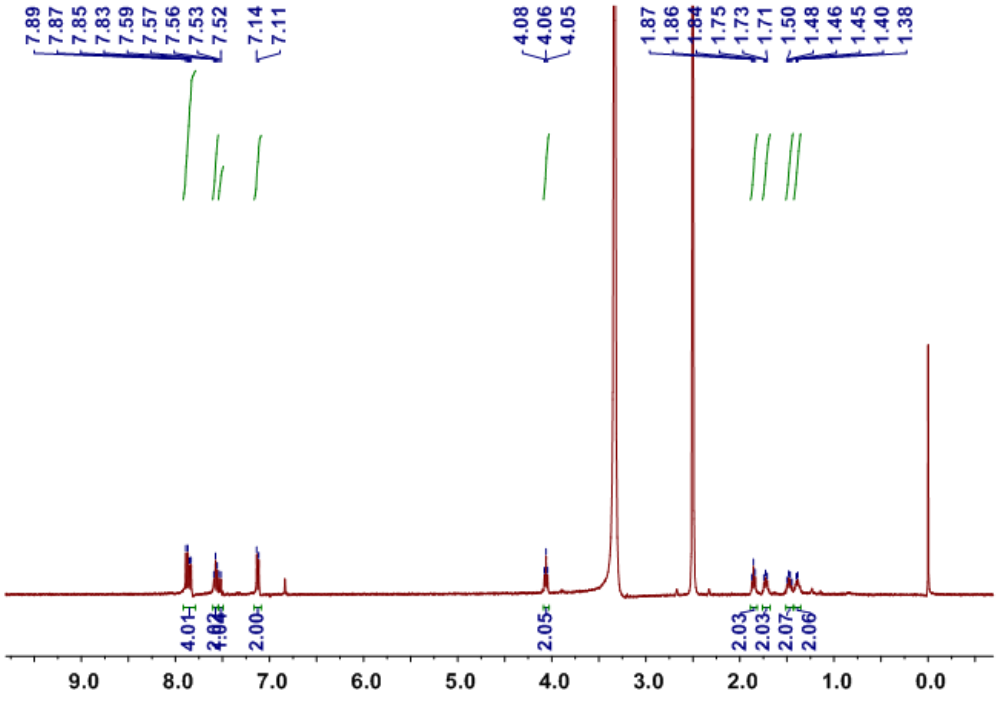

Fig. S4 ^{1}H NMR spectrum (400 MHz, DMSO-d_6, 293K) of **4**.

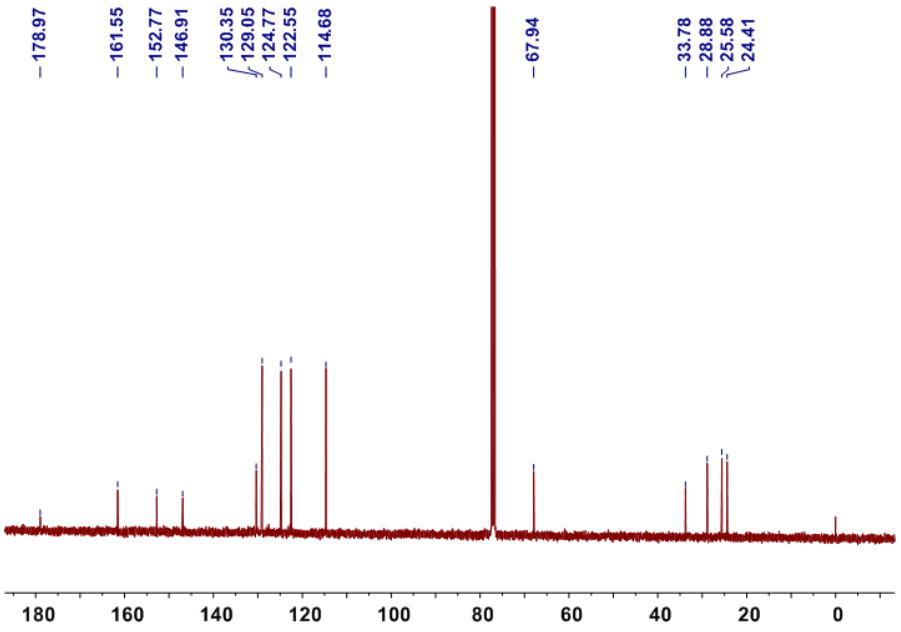

Figure S5 ^{13}C NMR spectrum (100 MHz, DMSO-d_6, 293K) of **4**.

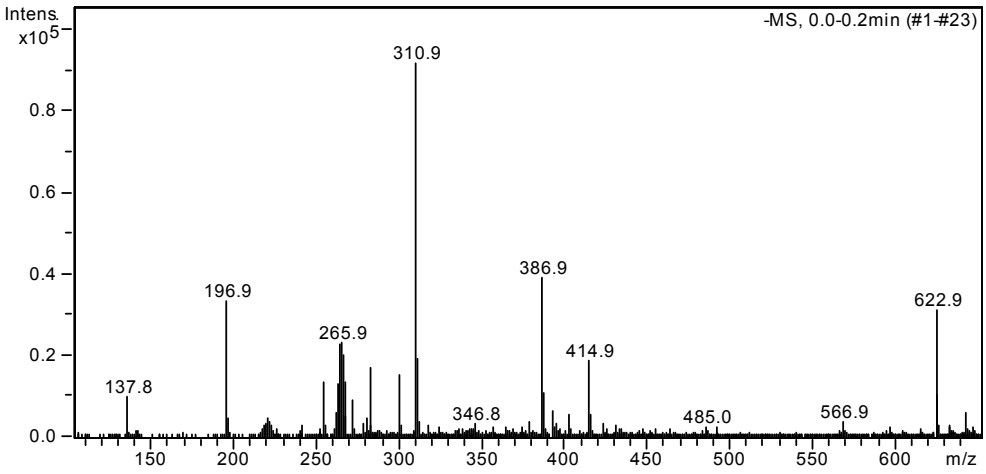

Fig. S6 Electrospray ionization mass spectrum of **4**. Assignment of the main peak: *m*/*z* 310.9 $[M - H]^-$.

Synthesis of 5. To a solution of **4** (1.56 g, 5.00 mmol) and *N,N′*-dimethylethanolamine (1.78 g, 20.0 mmol) in dry CH_2Cl_2 (100 mL), 4-dimethylaminopyridine (DMAP, catalytic amount) and 1-(3'-dimethylaminopropyl)-3-ethylcarbodiimide hydrochloride (EDC, 1.79 g, 10.0 mmol) were added under nitrogen atmosphere. The mixture was stirred overnight at room temperature. The solution was evaporated under vacuum and the residue was purified by flash column chromatography on silica gel (dichloromethane/petroleum ether = 2:1, *v*/*v*) to afford **5** as a red solid (1.53 g, 80%), mp 101.6−102.4 °C. The proton NMR spectrum of **5** is shown in Fig. S7. ^{1}H NMR (400 MHz, chloroform-*d*, room temperature) δ (ppm): 7.92–7.86 (m, 4H), 7.52 (t, J = 8.0 Hz, 2H), 7.43 (t, J = 8.0 Hz, 1H), 6.99 (d, J = 8.0 Hz, 2H), 4.18 (t, J = 8.0 Hz, 2H), 4.05 (t, J = 8.0 Hz, 2H), 2.56 (t, J = 8.0 Hz, 2H), 2.39 (t, J = 8.0 Hz, 2H), 2.28 (s, 6H), 2.37 (t, J = 8.0 Hz, 2H), 1.88–1.81 (m, 2H), 1.77–1.69 (m, 2H), 1.56–1.50 (m, 2H). The ^{13}C NMR spectrum of **5** is shown in Fig. S7. ^{13}C NMR (100 MHz, chloroform-*d*, room temperature)

δ (ppm): 173.53, 161.58, 152.73, 146.83, 130.30, 128.99, 124.74, 122.54, 114.65, 67.92, 62.00, 57.78, 45.65, 34.05, 28.83, 25.56, 24.61. LRESIMS is shown in Fig. S9: *m/z* 384.1 $[M + H]^+$ (100%). HRESIMS: *m/z* calcd for $[M + H]^+$ $C_{22}H_{30}N_3O_3$, 384.4840, found 384.4851, error 2.9 ppm.

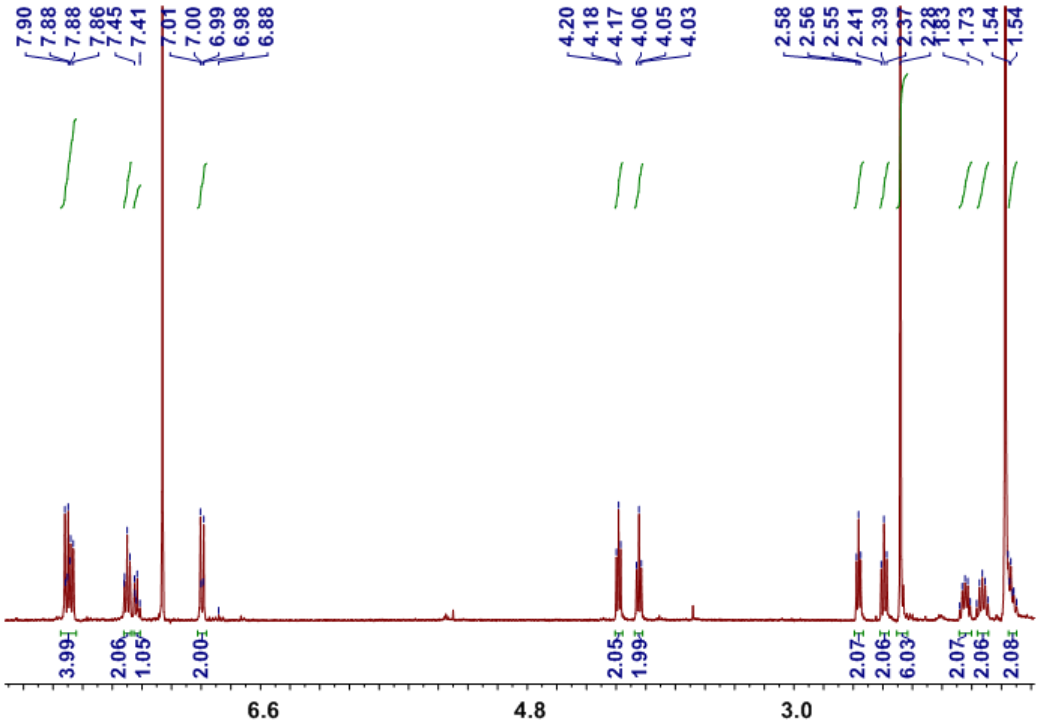

Fig. S7 ^{1}H NMR spectrum (400 MHz, chloroform-*d*, 293K) of **5**.

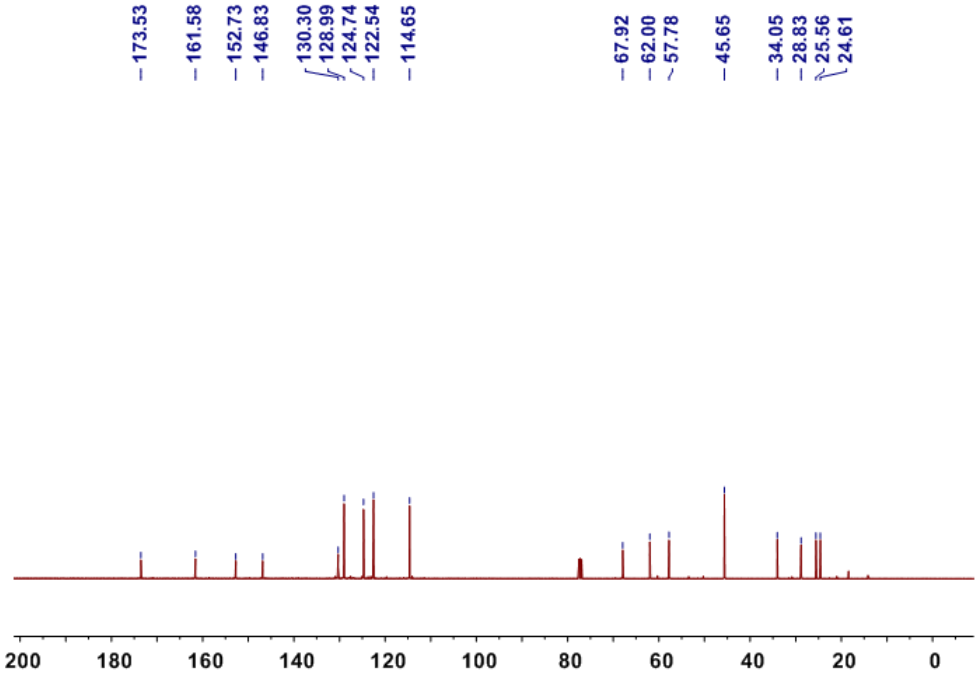

Fig. S8 ^{13}C NMR spectrum (100 MHz, chloroform-*d*, 293K) of **5**.

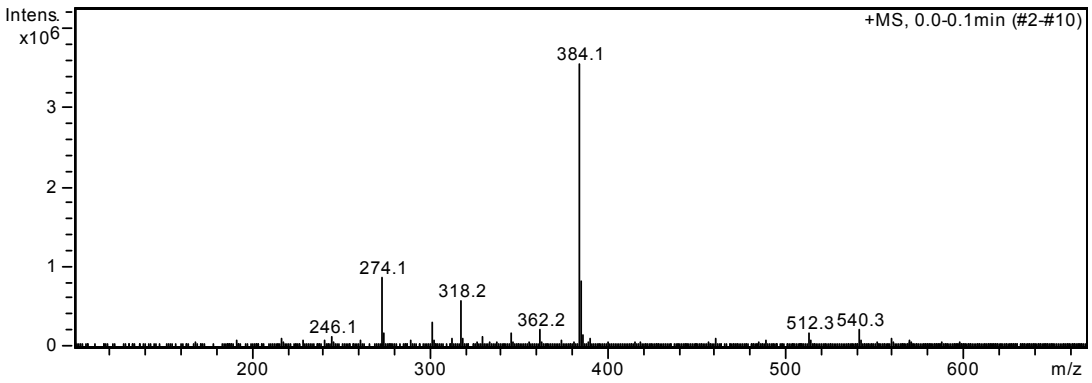

Fig. S9 Electrospray ionization mass spectrum of **5**. Assignment of the main peak: *m*/*z* 384.1 $[M + H]^+$.

Synthesis of AzoCh. A mixture of compound **5** (1.92 g, 5.00 mmol) and CH_3I (5.68 g, 40.0 mmol) was heated in *N,N*′-dimethylformamide (50 mL) at 50 °C for 12 h. The solvent was evaporated, and the residue was washed with CH_3OH to give **AzoCh** as a red solid (1.47 g, 56%), mp 109.4−110.5 °C. The proton NMR spectrum of **AzoCh** is shown in Fig. S10. ^{1}H NMR (400 MHz, DMSO-d_6, room temperature) δ (ppm): 7.91–7.84 (m, 4H), 7.60 (t, J = 8.0 Hz, 2H), 7.54 (t, J = 8.0 Hz, 1H), 7.12 (d, J = 8.0 Hz, 2H), 4.55 (t, J = 8.0 Hz, 2H), 4.09 (t, J = 8.0 Hz, 2H), 3.66 (t, J = 8.0 Hz, 2H), 3.13 (t, J = 8.0 Hz, 2H), 2.41 (t, J = 8.0 Hz, 2H), 1.81–1.74 (m, 2H), 1.68–1.60 (m, 2H), 1.51–1.44 (m, 2H). The ^{13}C NMR spectrum of **AzoCh** is shown in Fig. S11. ^{13}C NMR (100 MHz, DMSO-d_6, room temperature) δ (ppm): 172.28, 161.42, 151.97, 146.04, 130.80, 129.37, 124.57, 122.19, 115.01, 67.82, 63.73, 57.68, 52.92, 33.26, 28.22, 24.97, 23.90. LRESIMS is shown in Fig. S12: *m*/*z* 398.1 $[M - I]^+$ (100%). HRESIMS: *m*/*z* calcd for $[M - I]^+$ $C_{23}H_{32}N_3O_3$, 398.5179, found 398.5185, error 1.5 ppm.

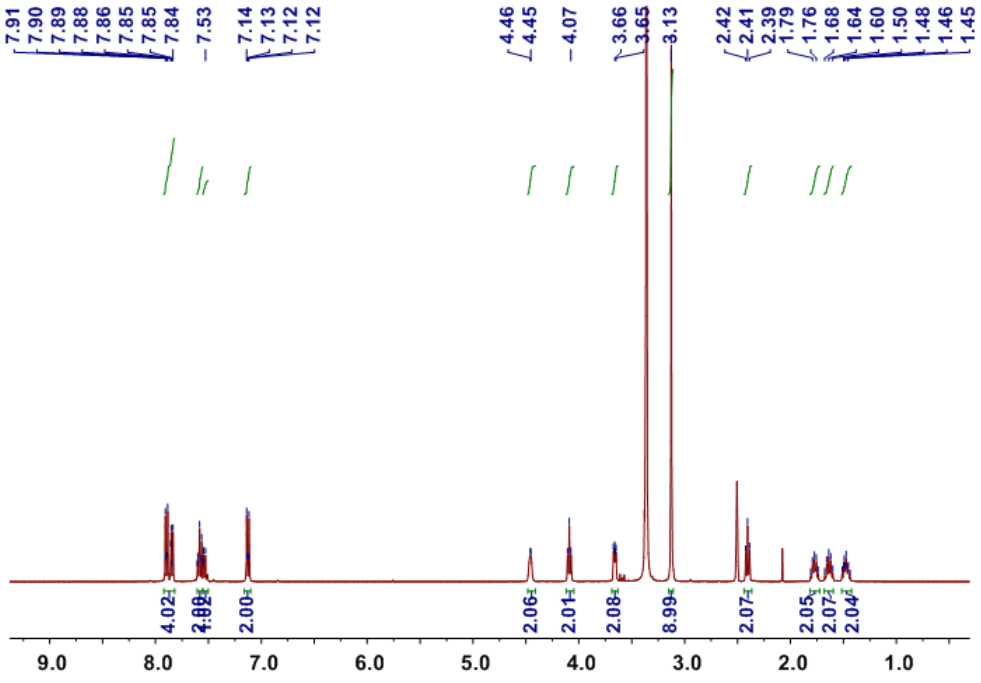

Fig. S10 ^{1}H NMR spectrum (400 MHz, DMSO-d_6, 293K) of **AzoCh**.

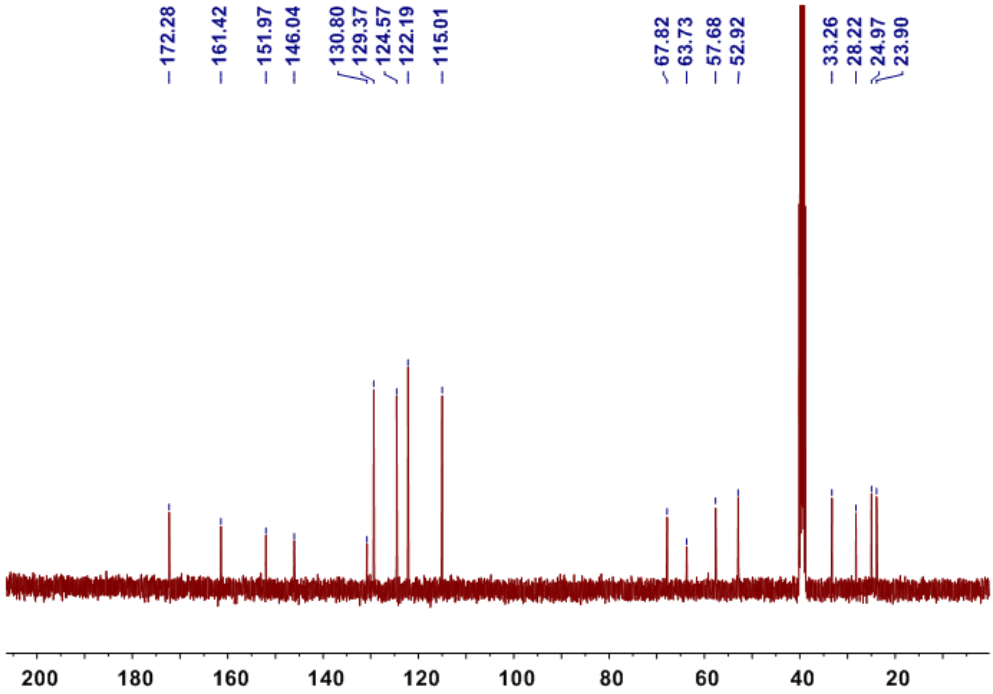

Fig. S11 ^{13}C NMR spectrum (100 MHz, DMSO-d_6, 293K) of **AzoCh**.

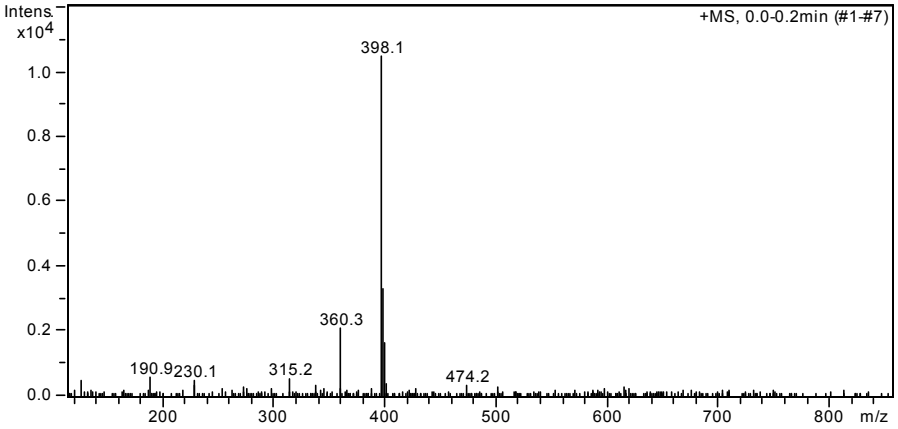

Fig. S12 Electrospray ionization mass spectrum of **AzoCh**. Assignment of the main peak: *m*/*z* 398.1 $[M - I]^+$.

*3. Host–guest complexation between **WP6** and butyrylcholine*

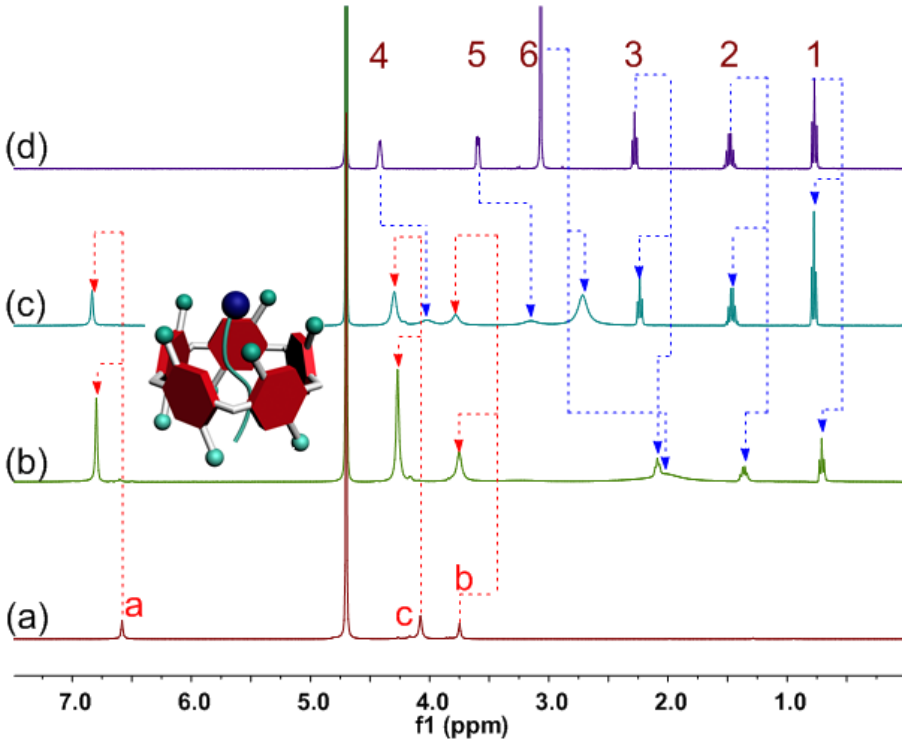

Fig. 13 Partial ^{1}H NMR spectra (400 MHz, D_2O, 293 K): (a) **WP6** (1.00 mM); (b) **WP6** (1.00 mM) and **M** (1.00 mM); (c) **WP6** (1.00 mM); (b) **WP6** (1.00 mM) and **M** (3.00 mM); (e) **M** (1.00 mM).

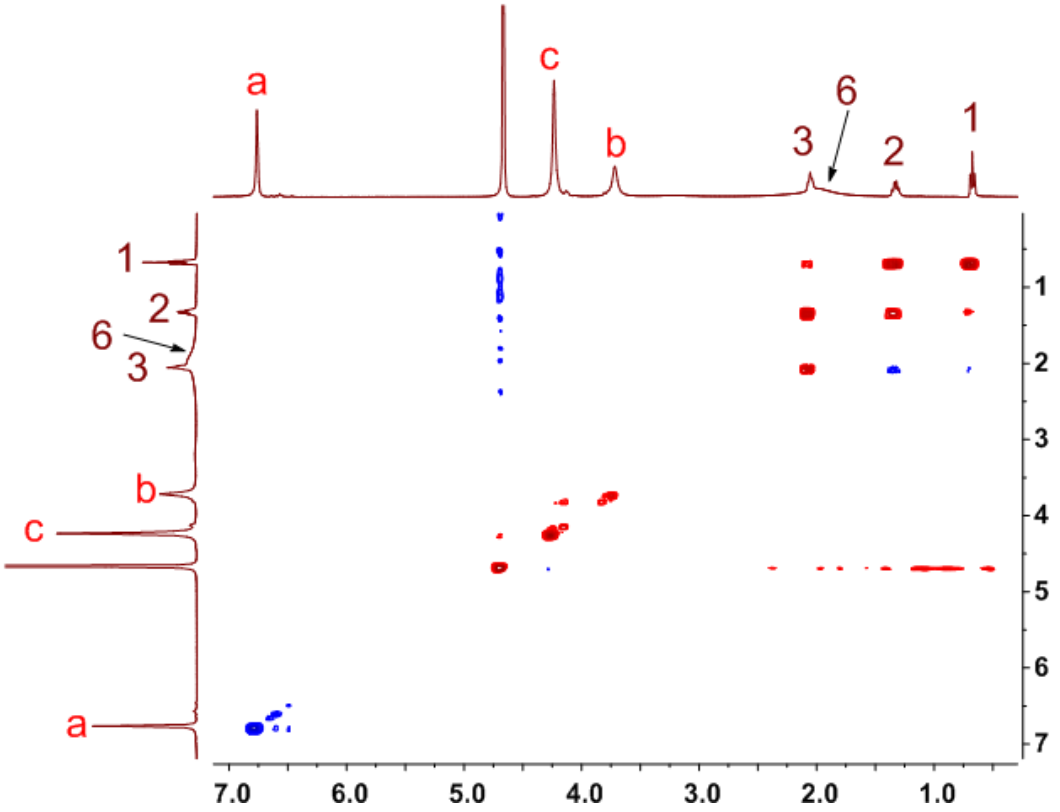

Fig. S14 2D COSY spectrum (500 MHz, D_2O, 295 K) of **WP6** (10.0 mM) and butyrylcholine (10.0 mM).

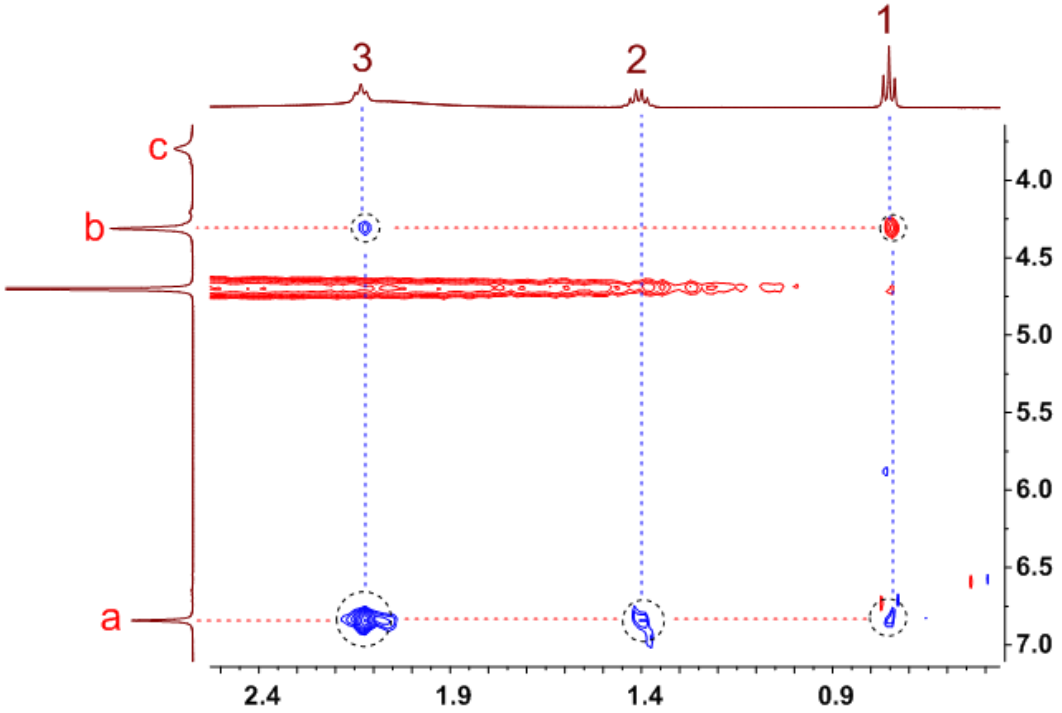

Fig. S15 2D NOESY spectrum (500 MHz, D_2O, 295 K) of **WP6** (10.0 mM) and butyrylcholine (10.0 mM).

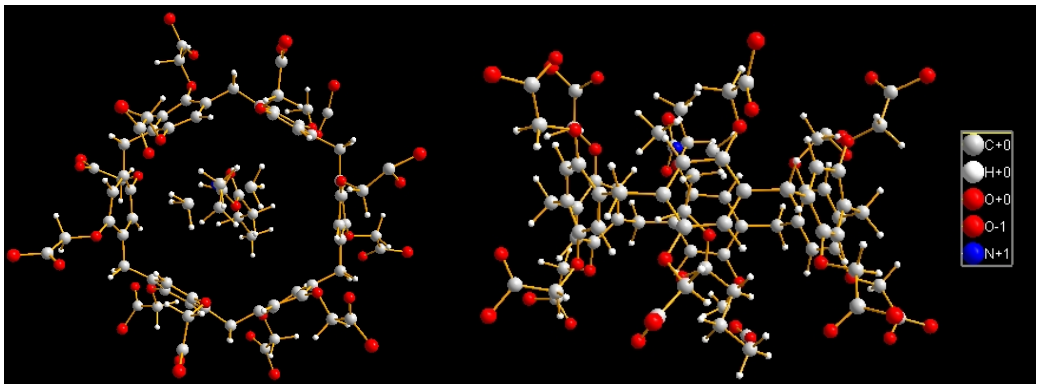

Fig. S16 Energy-minimized structure of **WP5**⊃butyrylcholine by the PM3 semiempirical molecular orbital method: (left) top view, (right) side view.

The molecular geometry optimization of **WP6**⊃**M** shows that the guest is tightly wrapped within **WP6**. Noticeably, the cationic segment of **M** is located on the upper side of **WP6** to successfully achieve multivalent electrostatic interactions with carboxylate groups on **WP6**, and the tail of **M** containing ester and methyl groups locates inside the cavity of **WP6**. The results obtained from 2D NOESY NMR spectroscopy and molecular modelling were in good agreement with each other, demonstrating that **M** deeply penetrated into the cavity of **WP6**, forming a 1:1 [2]pseudorotaxane-type host–guest inclusion complex.

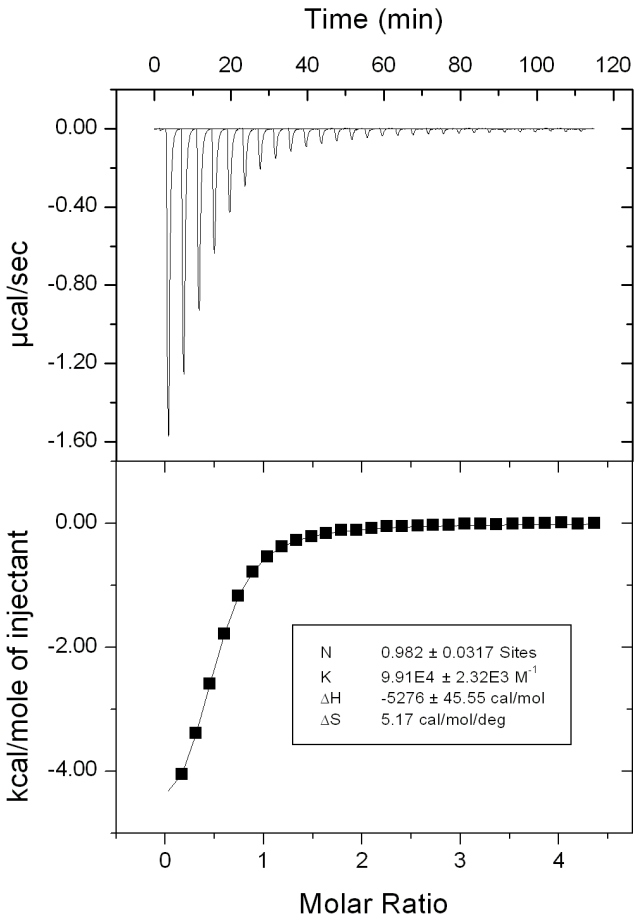

Fig. S17 Microcalorimetric titration of butyrylcholine with **WP6** in water at 298.15 K. (Top) Raw ITC data for 29 sequential injections (10 µL per injection) of a butyrylcholine solution (2.00 mM) into a **WP6** solution (0.100 mM). (Bottom) Net reaction heat obtained from the integration of the calorimetric traces.

4. Critical aggregation concentration (CAC) determination

Some parameters such as the conductivity, osmotic pressure, fluorescence intensity and surface tension of the solution change sharply around the critical aggregation concentration. The dependence of the solution conductivity on the solution concentration is used to determine the critical aggregation concentration. Typically, the slope of the change in conductivity versus the concentration below CAC is steeper than the slope above the CAC. Therefore, the junction of the conductivity-concentration plot represents the CAC value. To measure the CAC values of **AzoCh**, **WP6⊃AzoCh** and **WP6⊃AzoCh** in the presence of α-CD, the conductivities of the solutions at different concentrations were determined. By plotting the conductivity versus the concentration, we estimated the corresponding CAC values.

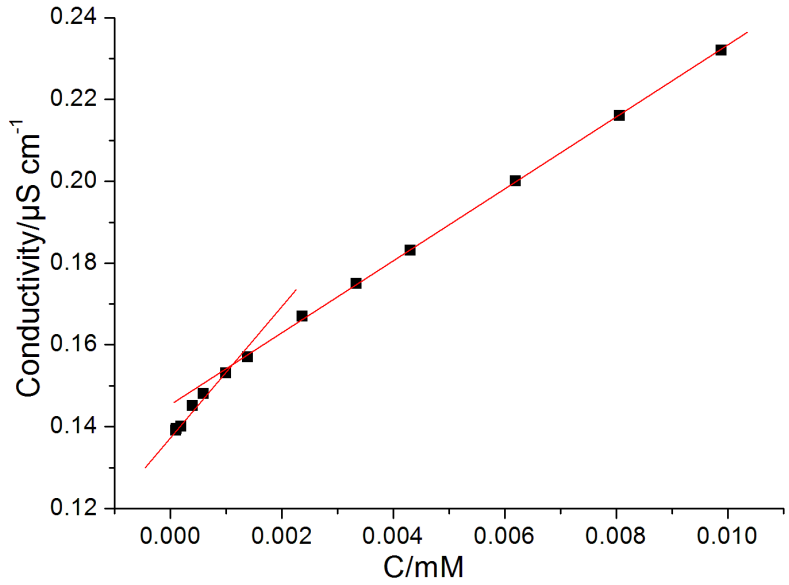

Fig. S18 The concentration-dependent conductivity of **AzoCh**. The critical aggregation concentration was determined to be 1.10×10^{-6} M.

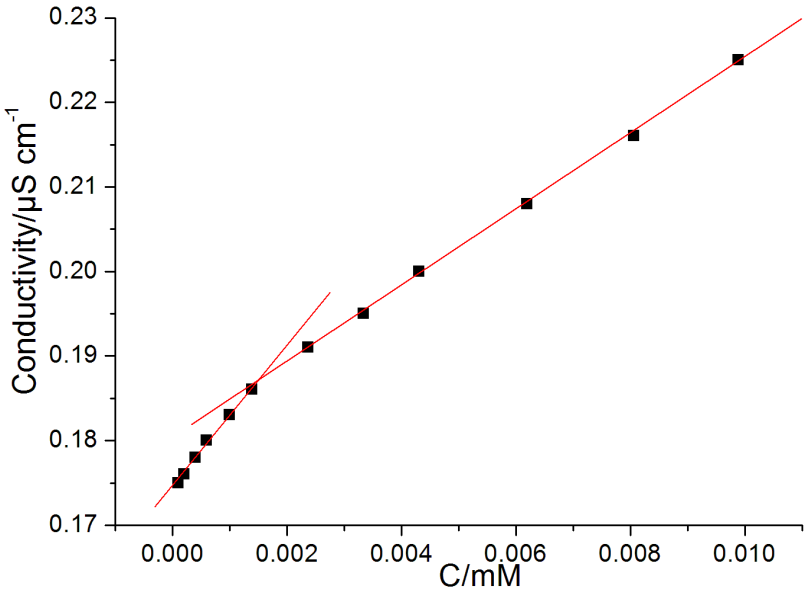

Fig. S19 The concentration-dependent conductivity of **AzoCh** upon UV irradiation. The critical aggregation concentration was determined to be 1.52×10^{-6} M.

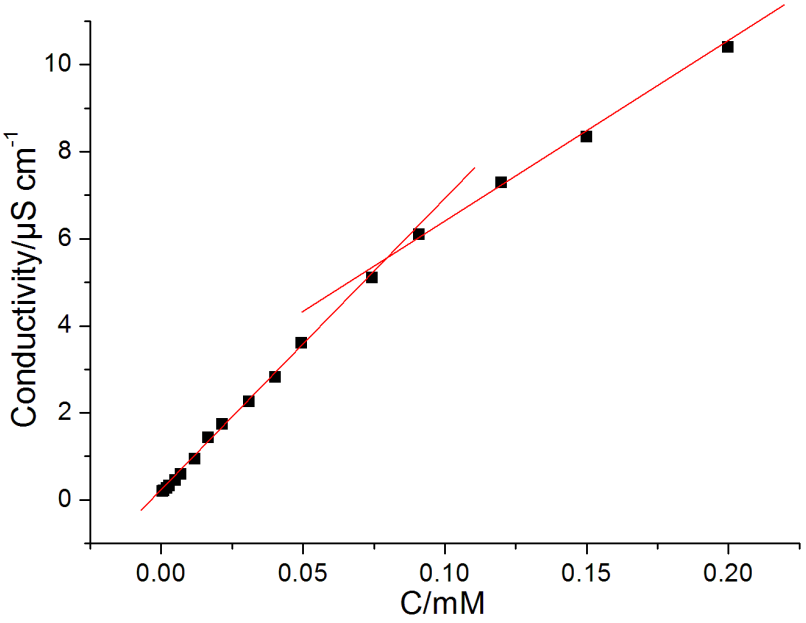

Fig. S20 The concentration-dependent conductivity of **WP6⊃AzoCh**. The critical aggregation concentration was determined to be 8.09×10^{-5} M.

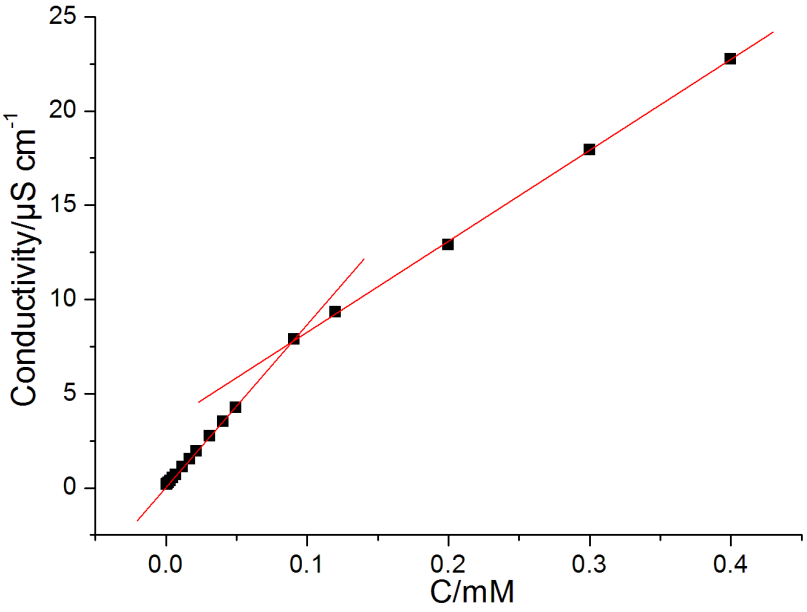

Fig. S21 The concentration-dependent conductivity of **WP6⊃AzoCh** upon UV irradiation. The critical aggregation concentration was determined to be 8.87×10^{-5} M.

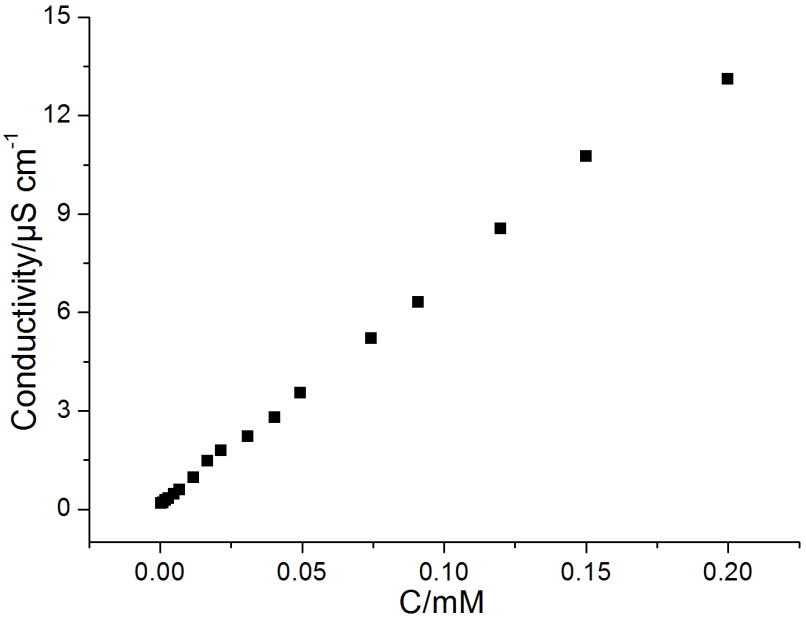

Fig. S22 The concentration-dependent conductivity of **WP6⊃AzoCh** in the presence of α-CD.

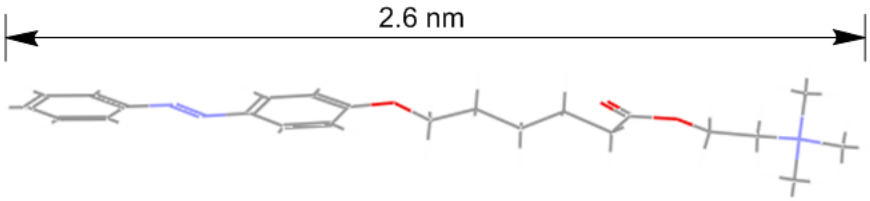

Fig. S23 The sizes (nm) of **AzoCh** obtained from PM3 semiempirical molecular orbital method.

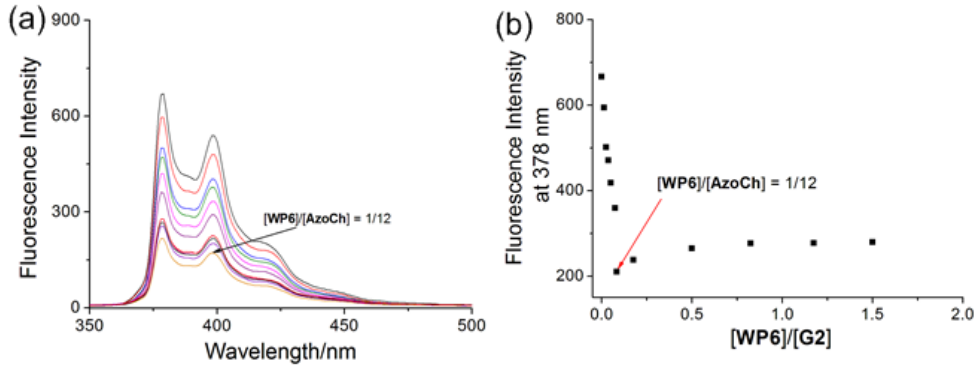

Fig. S24 (a) Fluorescence emission spectra of pyrene in aqueous solutions of **AzoCh** (0.0800 mM) by increasing the concentration of **WP6**. (b) Dependence of the relative fluorescence intensity of pyrene on **WP6** concentration with a fixed concentration of **AzoCh** (0.0800 mM). [pyrene] = 1.00 μM.

Figure S24a showed the absorbance evolution at 378 nm as a function of the **WP6** concentration with a fixed **AzoCh** concentration at 8.00×10^{-5} M. Upon gradual addition of **WP6**, the fluorescent intensity underwent a sharp decrease when the concentration of **WP6** reached 6.67×10^{-6} M. Then, an inverse increase was observed upon further addition of **WP6**. The inflection appears when the **WP6**/**AzoCh** molar ratio is 1/12 (Figure S13b). In the

left-hand portion of inflection, **WP6** and **AzoCh** form a higher-order complex with a tendency toward supramolecular amphiphilic aggregation, whereas in the right-hand portion of inflection, excess **WP6** in solution leads to the formation of a simple 1:1 inclusion complex rather than higher-order aggregation.[S2]

5. DLS determinations of the vesicles size

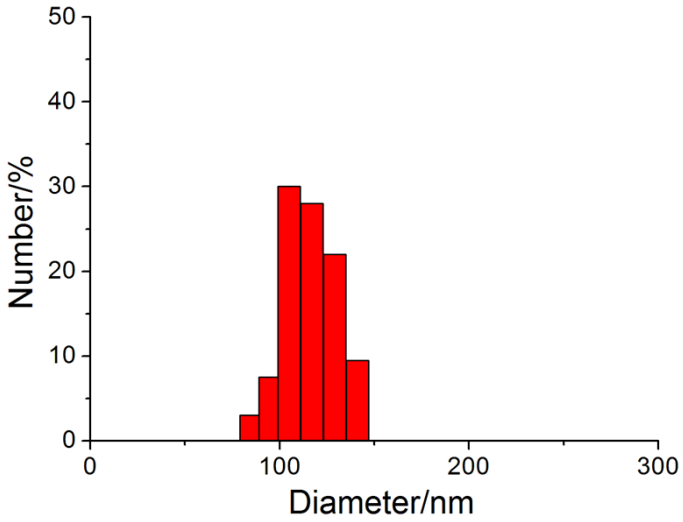

Fig. S25 DLS result of **WP6⊃AzoCh**. The average diameter of the vesicles was determined to be 138 nm.

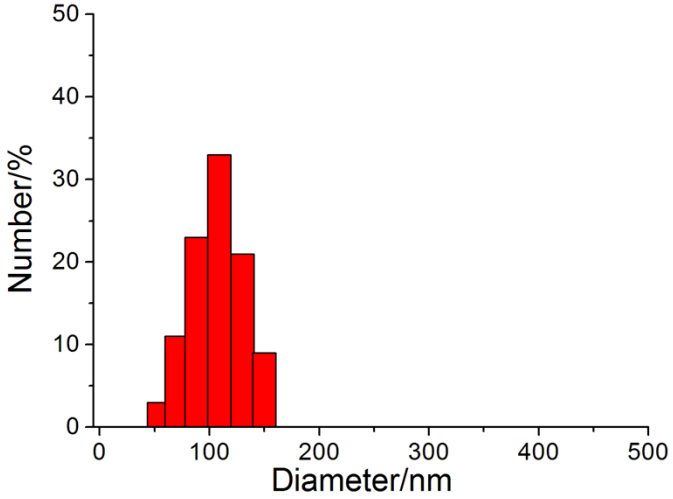

Fig. S26 DLS result of **WP6⊃AzoCh** upon UV irradiation. The average diameter of the vesicles was determined to be 109 nm.

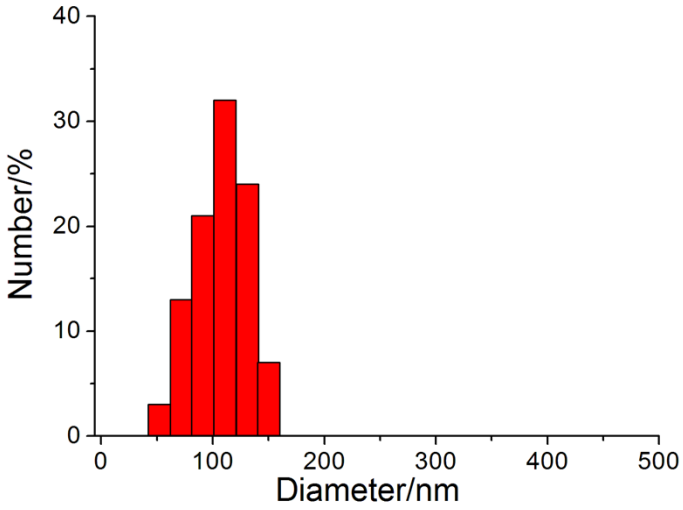

Fig. S27 DLS result of **WP6⊃AzoCh** in the presence of *α*-CD upon UV irradiation. The average diameter of the vesicles was determined to be 116 nm.

*6. The photoisomeric behaviors of **AzoCh***

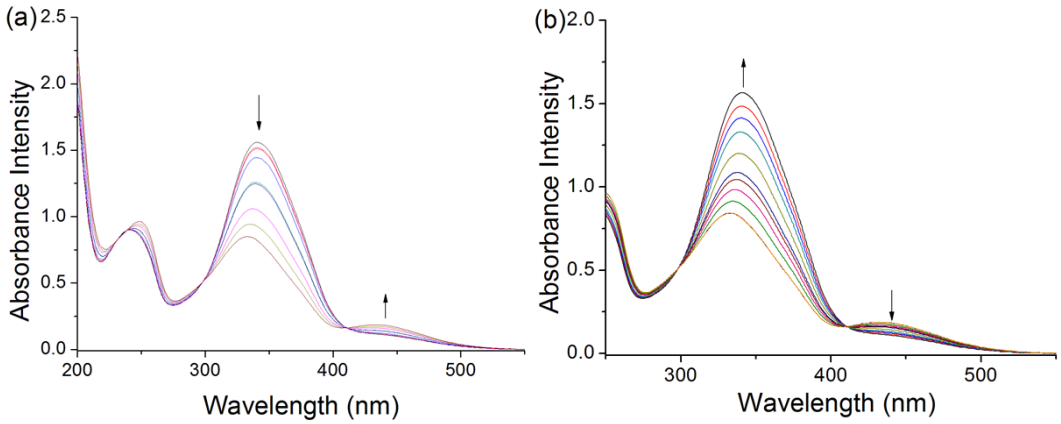

Fig. S28 UV-Vis absorption spectra of **AzoCh** under UV irradiation at 365 nm (a) and later after visible irradiation at 435 nm (b).

As expected, **AzoCh** exhibited good photoresponsive properties as investigated by UV-Vis spectroscopy (Figure S22). Upon irradiation with UV light at 365 nm, the absorption band at around 335 nm decreased remarkably, and concomitantly the band at around 430 nm increased slightly. The absorption bands of the azobenzene unit at 335 and 430 nm are ascribed to π-π* and n-π* transitions, respectively. The changes of the absorption bands induced by UV irradiation indicated the photoisomerization from the *trans*-**AzoCh** state to the *cis*-**AzoCh** state. On the contrary, upon irradiation with visible light at 435 nm, the absorption peak at 430 nm attributable to *cis*-**AzoCh** decreased, while the absorption band at 335m corresponding to *trans*-**AzoCh** increased, indicating a change from the *cis*-**AzoCh** form to the *trans*- **AzoCh** form.

7. Mass spectroscopy measurements

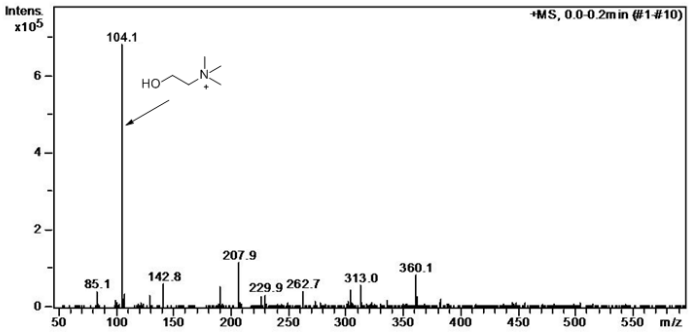

Fig. S29 Electrospray ionization mass spectrum (positive) of **AzoCh** upon treatment of AChE for 24 h.

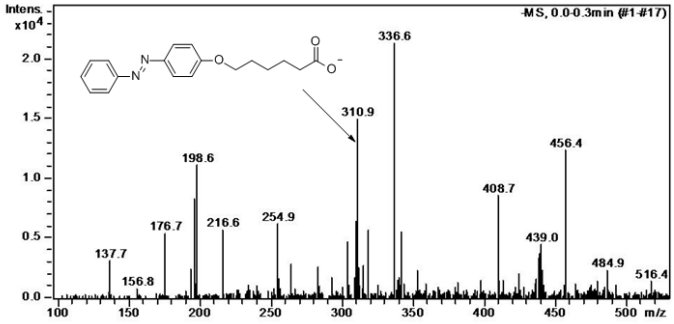

Fig. S30 Electrospray ionization mass spectrum (negative) of **AzoCh** upon treatment of AChE for 24 h. Assignment of the main peak: *m*/*z* 310.9 [**AzoH** – H]$^-$.

8. Controllable release of calcein from the vesicles in response to different stimuli

Calcein, a common hydrophilic dye and an excellent UV/vis and fluorescence probe that could be encapsulated by the vesicles, was used as a dye molecule to investigate the controlled release behavior in response to the external-stimuli (acidation solution pH, addition of α-CD and treatment with enzyme). When the vesicles were destroyed, the encapsulated calcein is released out and the fluorescence intensity of its aqueous solution increased

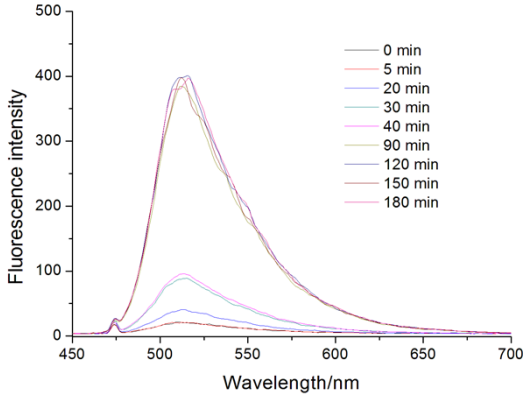

Fig. S31 Fluorescence emission spectra at different time after acidation the solution pH to 6.0.

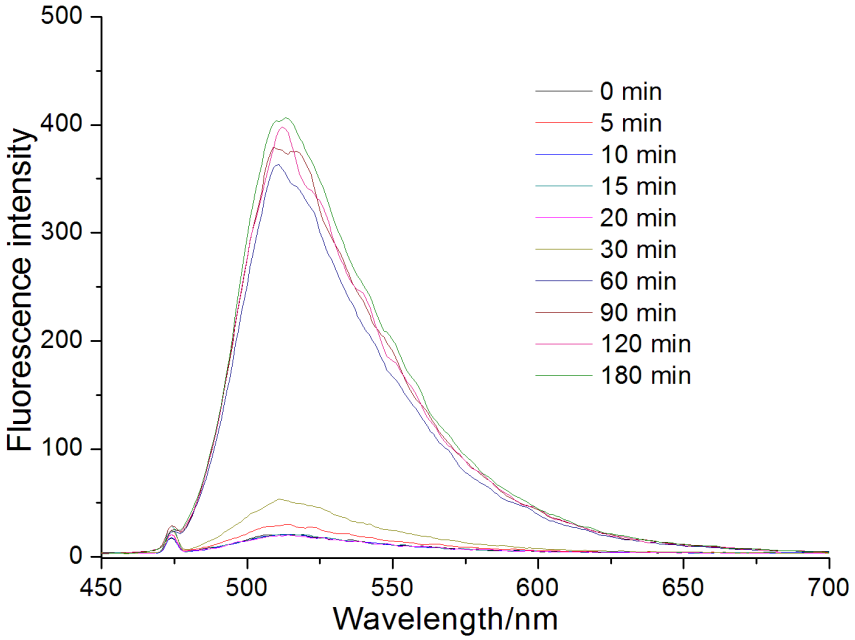

Fig. S32 Fluorescence emission spectra at different time upon addition of α-CD.

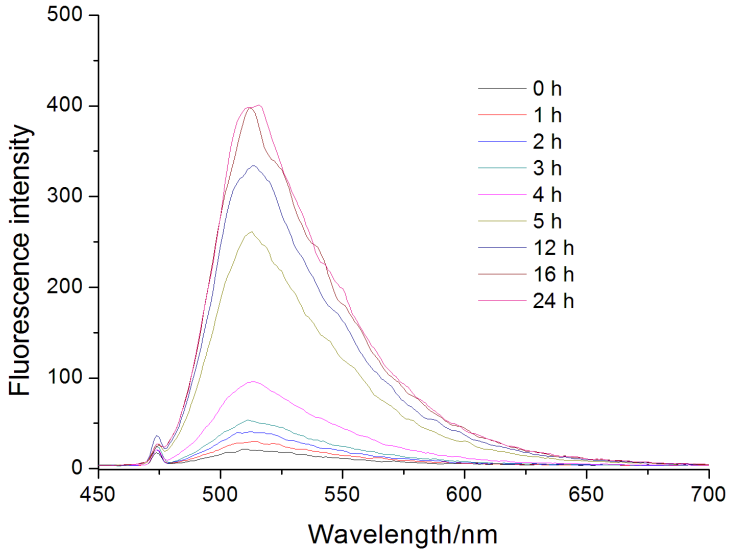

Fig. S33 Fluorescence emission spectra at different time upon addition of AChE (6 U/mL).

9. *TEM images of the self-assemblies*

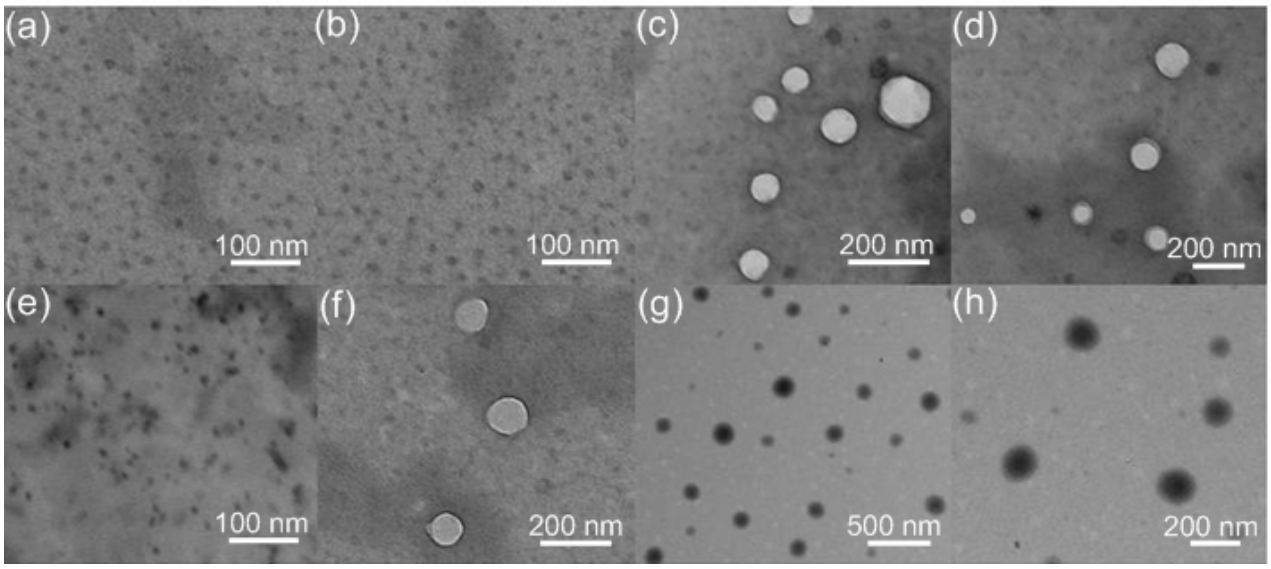

Fig. S34 TEM images: (a) **AzoCh**, (b) **AzoCh** after irradiation with UV light (365 nm, 8W), (c) **WP6⊃AzoCh**, (d) **WP6⊃AzoCh** after irradiation with UV light (365 nm, 8W), (e) **WP6⊃AzoCh** when the solution pH was adjusted to 6.0, (f) **WP6⊃AzoCh** in the presence of *α*-CD after irradiation with UV light (365 nm, 8W), (g) **WP6⊃AzoCh** after culturing with AChE for 24 h, (h) enlarged image of (g).

References:

S1. G. Yu, X. Zhou, Z. Zhang, C. Han, Z. Mao, C, Gao and F. Huang, *J. Am. Chem. Soc.*, 2012, **134**, 19489–19497.

S2. G. Yu, X. Zhou, Z. Zhang, C. Han, Z. Mao, C. Gao and F. Huang, *J. Am. Chem. Soc*., 2012, **134**, 19489–19497.